5644–5656 *Nucleic Acids Research, 2014, Vol. 42, No. 9* *Published online 12 March 2014*
doi: 10.1093/nar/gku190

The DNA damage checkpoint pathway promotes extensive resection and nucleotide synthesis to facilitate homologous recombination repair and genome stability in fission yeast

Elizabeth J. Blaikley[1,*], Helen Tinline-Purvis[1,*], Torben R. Kasparek[1], Samuel Marguerat[2,†], Sovan Sarkar[1], Lydia Hulme[1], Sharon Hussey[1], Boon-Yu Wee[1], Rachel S. Deegan[1], Carol A. Walker[1], Chen-Chun Pai[1], Jürg Bähler[2], Takuro Nakagawa[3] and Timothy C. Humphrey[1,‡]

[1]CRUK-MRC Gray Institute for Radiation Oncology and Biology, University of Oxford, OX3 7DQ, UK, [2]Department of Genetics, Evolution and Environment, and UCL Cancer Institute, University College London, London WC1E 6BT, UK, and [3]Department of Biological Sciences, Graduate School of Science, Osaka University, Toyonaka 560-0043, Osaka, Japan

Received August 29, 2013; Revised February 18, 2014; Accepted February 19, 2014

ABSTRACT

DNA double-strand breaks (DSBs) can cause chromosomal rearrangements and extensive loss of heterozygosity (LOH), hallmarks of cancer cells. Yet, how such events are normally suppressed is unclear. Here we identify roles for the DNA damage checkpoint pathway in facilitating homologous recombination (HR) repair and suppressing extensive LOH and chromosomal rearrangements in response to a DSB. Accordingly, deletion of Rad3^{ATR}, Rad26^{ATRIP}, Crb2^{53BP1} or Cdc25 overexpression leads to reduced HR and increased break-induced chromosome loss and rearrangements. We find the DNA damage checkpoint pathway facilitates HR, in part, by promoting break-induced Cdt2-dependent nucleotide synthesis. We also identify additional roles for Rad17, the 9-1-1 complex and Chk1 activation in facilitating break-induced extensive resection and chromosome loss, thereby suppressing extensive LOH. Loss of Rad17 or the 9-1-1 complex results in a striking increase in break-induced isochromosome formation and very low levels of chromosome loss, suggesting the 9-1-1 complex acts as a nuclease processivity factor to facilitate extensive resection. Further, our data suggest redundant roles for Rad3^{ATR} and Exo1 in facilitating extensive resection. We propose that the DNA damage checkpoint pathway coordinates resection and nucleotide synthesis, thereby promoting efficient HR repair and genome stability.

INTRODUCTION

DNA double-strand breaks (DSBs) are potentially lethal lesions, which can arise from exposure to DNA damaging agents or through endogenous metabolic errors. DSBs are normally efficiently repaired by the non-homologous end-joining (NHEJ) or homologous recombination (HR) repair pathways. However, incorrectly repaired DSBs can give rise to a wide range of chromosomal rearrangements, which can lead to oncogene activation or tumor suppressor loss through loss of heterozygosity (LOH) (reviewed in (1)).

The DNA damage checkpoint pathway plays a key role in maintaining genome stability in response to DNA damage. While originally identified as an intracellular signal transduction pathway that detects DNA lesions and blocks cell cycle progression until DNA repair is completed (2), the DNA damage checkpoint pathway is now understood to promote genome stability through a wide range of processes including transcriptional regulation of repair genes (3); regulation of nucleotide synthesis (4); interaction with, and post-translational modification of DNA repair proteins (5); relocalization of repair proteins (6) and regulation of the formation of DNA repair centres (7) (reviewed in (8)).

Central to the DNA damage checkpoint are the phosphatidylinositol 3′ kinase-like kinases, ataxia telangiectasia mutated (ATM) in humans (*Hs*) (Tel1 in *Schizosaccharomyces pombe* (*Sp*) and *Saccharomyces cerevisiae* (*Sc*)) and ataxia telangiectasia and Rad3-related ATR^{Hs}

*These authors contributed equally to this work.
The authors wish it to be known that, in their opinion, the first two authors should be regarded as Joint First Authors.
†Present address: MRC Clinical Sciences Centre, Imperial College London, London W12 0NN, UK
‡To whom correspondence should be addressed. Tel: +44 1865 617327; Fax: +44 1865 617318; Email: timothy.humphrey@oncology.ox.ac.uk

(Rad3^{Sp}/Mec1^{Sc}), which localize to DNA damage and play important roles as the initial sensor kinases (9). During checkpoint activation, the checkpoint loading complex, a modified form of the replication factor C (RFC) heteropentamer in which the Rfc1 subunit is replaced by a checkpoint-specific subunit Rad17$^{Sp/Hs}$ (Rad24^{Sc}), recognizes single-stranded DNA (ssDNA)/double-stranded DNA junctions generated at damage sites (10,11). This recruits the 9-1-1 checkpoint sliding clamp complex, a heterotrimer composed of Rad9$^{Sp/Hs}$, Hus1$^{Sp/Hs}$, Rad1$^{Sp/Hs}$ (Ddc1^{Sc}, Mec3^{Sc} and Rad17^{Sc}), which structurally resembles proliferating cellnuclear antigen (PCNA), the processivity factor for DNA replication (12–14). Both the Rad17 checkpoint loading complex and the 9-1-1 complex are required for activation of the ATR^{Hs}/Rad3^{Sp}/Mec1^{Sc} checkpoint kinase. The ATR^{Hs}/Rad3^{Sp}/Mec1^{Sc} kinase is recruited through its interaction between ATRIP^{Hs}/Rad26^{Sp}/Ddc2^{Sc} and replication protein A (RPA) (15), and colocalization of Ddc1^{Sc} with Mec1^{Sc} is necessary and sufficient for checkpoint activation (16).

The checkpoint signal is transduced through recruitment and activation of the effector kinases, Chk1$^{Sp/Hs/Sc}$ and Chk2^{Hs}/Cds1^{Sp}/Rad53^{Sc}. This is achieved through ATR^{Hs}/Rad3^{Sp}/Mec1^{Sc}-dependent phosphorylation of the checkpoint clamp Rad9$^{Sp/Hs}$/Ddc1^{Sc} and recruitment of TopBP1^{Hs}/Rad4/Cut5^{Sp}/Dpb11^{Sc} (17,18). Effector kinase activity is regulated by mediator proteins. In fission yeast, activation of Chk1 in response to DNA damage is mediated by Crb2^{53BP1}, while activation of Cds1^{Chk2} kinase in response to replication stress is mediated by Mrc1 (19–21).

The cell cycle is subsequently targeted by the checkpoint effector kinases. In fission yeast, Cdc25 is phosphorylated by Chk1 or Cds1^{Chk2} in response to DNA damage or replication stress, respectively (22,23). This results in Cdc25 nuclear export through the binding of Rad24, a 14-3-3 protein, thus preventing activation of nuclear Cdc2^{CDK1} kinase, thereby resulting in G2 arrest (24,25). Accordingly, checkpoint inactivation can be achieved through overexpression of Cdc25 (26).

In agreement with a central role for the DNA damage checkpoint in maintaining genome stability, its disruption has been shown to result in elevated levels of spontaneous and break-induced chromosomal rearrangements in both yeast and humans (27–32). Further, DNA damage checkpoint genes have been shown to function as tumor suppressors, in accordance with their role in maintaining genome stability (33). Despite a reasonable understanding of DNA damage checkpoint signalling, less is known about how this pathway coordinates repair in response to DNA damage.

In this study, we have examined the roles of the DNA integrity checkpoint genes in facilitating DSB repair and genome stability in fission yeast. We show that loss of the DNA damage checkpoint can lead to strikingly increased levels of break-induced chromosomal rearrangements and extensive LOH. Our findings identify distinct roles for DNA damage checkpoint genes in promoting efficient HR and genome stability in response to a DSB through both facilitating nucleotide synthesis and extensive resection.

MATERIALS AND METHODS

Yeast strains, media and genetic methods

All *S. pombe* strains were cultured, manipulated and stored as previously described (34). All strain genotypes are listed in Supplementary Table S1. The construction of Ch^{16}-RMGAH is as described in (35).

Serial dilution assays

Log phase cultures of OD 0.2 (595 nm) of the strains indicated were spotted onto Ye5S plates with the indicated concentrations of bleocin. Plates were incubated at 32°C for two days before analysis.

Site-specific DSB assay

The DSB assay was performed as described previously (34). The percentage of colonies undergoing NHEJ/SCC (arg$^+$ G418^R/Hyg^R ade$^+$ his$^+$), gene conversion (GC) (arg$^+$ G418^S/Hyg^S ade$^+$ his$^+$), Ch^{16} loss (arg$^-$ G418^S/Hyg^S ade$^-$ his$^-$) or LOH (arg$^+$ G418^S/Hyg^S ade$^-$ his$^-$; Hyg^R ade$^-$ G418^S his$^-$ for Ch^{16}-YAMGH) were calculated. To determine the levels of break-induced GC, Ch^{16} loss and LOH, background events at 48h-T in a blank vector assay were subtracted from break-induced events at 48h-T in cells transformed with pREP81X-HO. Each experiment was performed three times using three independently derived strains for all mutants tested. More than 1000 colonies were scored for each time point. Southern blots were performed as previously described (34). It has been previously estimated that every cell will have incurred at least one HO endonuclease-induced DSB during this assay (36).

Rapidly inducible DSB resection and SSA repair assay

Rapid HO induction using the *urg* promoter together with analysis of DSB resection and single-strand annealing (SSA) repair was performed as previously described (37,38).

Pulsed field gel electrophoresis

Pulsed field gel electrophoresis (PFGE) analysis was performed as described previously (39).

Comparative genome hybridization

Comparative genome hybridization (CGH) analysis was performed as previously described (35).

RESULTS

Rad3^{ATR} is a suppressor of break-induced LOH

To identify suppressors of break-induced LOH, a colony-sectoring screen was performed following ethyl methanesulfonate (EMS) mutagenesis of a strain carrying a modified non-essential minichromosome (Ch^{16}-RMGAH). Ch^{16}-RMGAH encodes an *arg3* marker on the left arm of the minichromosome, and a *MATa* target site, together with an adjacent *kanMX6* gene encoding G418 resistance, an *ade6-M216*, allele which complements the *ade6-M210* allele

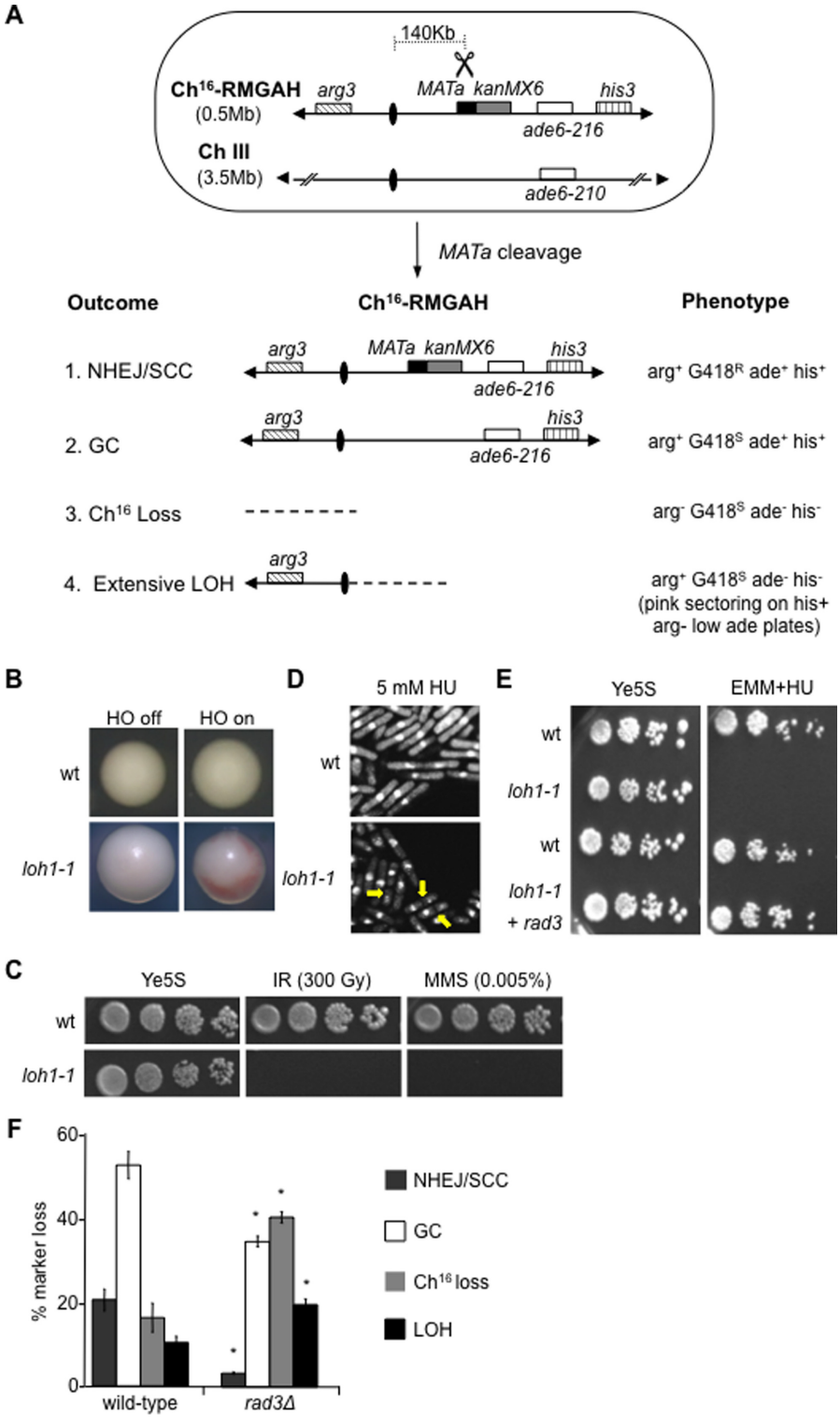

Figure 1. Rad3^{ATR} suppresses break-induced extensive LOH. (**A**) Schematic of the minichromosome Ch^{16}-RMGAH. The relative positions of the *arg3* marker (diagonal stripes), centromeres (ovals), the *MATa* site (black), the *kanMX6* resistance marker (gray), the complementary *ade6* heteroalleles (*ade6-M216* and *ade6-M210*; white) and the *his3* marker (vertical stripes) on Ch^{16}-RMGAH and ChIII are shown as described previously (35). The sizes of the ChIII and Ch^{16} are shown. In Ch^{16}-RMYAH, *kanMX6* is replaced by *hph*. Derepression of pREP81X-HO (not shown) generates a DSB at the *MATa* target site (scissors). Possible outcomes resulting from DSB induction, together with schematics of the minichromosome, and expected phenotypes are shown. (**B**) Colony sectoring of wild-type or *loh1–1* arg$^+$ G418^S ade$^-$ his$^-$ colonies grown on Edinburgh minimal medium (EMM) plus uracil, histidine and low adenine (5 mg/l) without arginine (arg- plates) thus facilitating detection of extensive LOH (LOH) in the presence (HO off) or absence (HO on) of thiamine. (**C**) Ten-fold serial dilutions of wild-type (WT) Ch^{16}-RMGAH (TH2130) or *loh1–1* (TH4089) strains on Ye5S plates, Ye5S plates exposed to 300 Gy IR, or 0.005% MMS as indicated. (**D**) 4',6-diamidino-2-phenylindole (DAPI) stained wild-type Ch^{16}-RMGAH (TH2130) or *loh1–1* (TH4089) strains either untreated or following exposure to 5 mM HU for 6 h. 'Cut' phenotypes indicated (yellow arrows). (**E**) Serial dilutions of wild-type Ch^{16}-RMGAH (TH2130), *loh1–1* (TH4089) with pREP41X empty vector or pREP41X-*rad3* (TH4093) on Ye5S and 10 mM HU EMM plates without thiamine, to derepress pREP41X expression. (**F**) Percentage DSB-induced marker loss of Ch^{16}-RMGAH in wild-type (TH2130) and *rad3Δ* (TH2941) backgrounds. The levels of NHEJ/sister chromatid conversion (SCC), GC, Ch^{16} loss and extensive LOH are shown. Data are the mean of three experiments and standard errors of the mean are indicated. The asterisk (*) represents significant difference compared to wild-type.

present on the homologous chromosome ChrIII, and a *his3* marker on the right arm (Figure 1A). These cells are heterozygous for these markers. Following HO endonuclease-induced cleavage at the *MATa* site, extensive break-induced LOH resulting from loss of the distal chromosome arm would be expected to result in arg^+ $G418^S$ ade^- his^- cells, which can be detected when occurring at increased levels as pink sectored colonies when grown on arg- plates in the presence of low levels of adenine (35) (Supplementary Figure S1). Following mutagenesis of the strain carrying Ch^{16}-RMGAH, mutants *loh1-loh7* exhibited elevated levels of break-induced sectoring and were isolated from the screen. The mutants *loh2-1*, *loh3-1* and *loh4-1* corresponded to mutations in *rad57*$^+$, *rad52*$^+$ and *rad51*$^+$, respectively, as previously described (35); our unpublished results.

Here we investigated the mutant *loh1-1* and found it exhibited increased break-induced sectoring (Figure 1B), and acute sensitivity to ionizing radiation (IR), and methyl methanesulfonate (MMS) (Figure 1C). Further analysis indicated *loh1-1* exhibited a 'cut' (cells untimely torn) phenotype in the presence of hydroxyurea (HU), which depletes nucleotide pools and disrupts DNA replication (Figure 1D). A 'cut' phenotype can arise from a DNA integrity checkpoint defect in which instead of arresting mitosis prior to the completion of DNA replication, unreplicated DNA is divided into two daughter cells (26). These findings strongly suggested *loh1-1* encoded a mutation in a checkpoint gene. Accordingly, a cross between *rad3Δ* and *loh1-1* was unable to generate progeny with wild-type sensitivity to DNA damaging agents, and the HU sensitivity of *loh1-1* could be rescued by expression of a plasmid encoding *rad3* (Figure 1E). Sequence analysis confirmed *loh1-1* encoded a W1700X mutation in the *rad3*$^+$ gene, in which a stop codon was introduced. This mutation lies in the FRAP-ATM-TRRAP (FAT) domain, a kinase domain that is conserved through the phosphatidylinositol 3-kinase-related kinase family (40). Similar findings were obtained for *loh5-1* and *loh7-1,* which were found to encode W1701X and W253X mutations in the *rad3*$^+$ gene (our unpublished results).

To further assess the role of $Rad3^{ATR}$ in suppressing break-induced LOH, a DSB assay was performed to quantitate levels of marker loss in a *rad3Δ* background compared to wild-type following break induction in a non-essential minichromosome. Following HO endonuclease-induced cleavage at the *MATa* site in a wild-type strain carrying Ch^{16}-RMGAH, 20.5% of cells were repaired by NHEJ or sister chromatid conversion (SCC) and maintained all the minichromosome markers (arg^+ $G418^R$ ade^+ his^+); 52.7% of cells were repaired by interchromosomal GC leading to loss of the $G418^R$ cassette adjacent to the break site on the minichromosome (arg^+ $G418^S$ ade^+ his^+); 16.3% of colonies failed to repair the break and lost the non-essential minichromosome (arg^- $G418^S$ ade^- his^-) and 10.3% underwent break-induced extensive LOH resulting in loss of the distal minichromosome arm (arg^+ $G418^S$ ade^- his^-) (Figure 1A and F).

DSB induction in a *rad3Δ* background confirmed a role for $Rad3^{ATR}$ in both promoting efficient HR repair and suppressing Ch^{16} loss and break-induced LOH, as previously described (44). The *rad3Δ* strain exhibited significantly reduced NHEJ/SCC (3.3% $P = 0.01$) and GC (34.7% $P = 0.02$) compared to wild-type. This was accompanied by a significant increase in both Ch^{16} loss (40.5% $P < 0.01$) and break-induced extensive LOH (19.6% $P < 0.01$) (Figure 1F). No significant loss of viability was observed following DSB induction in this non-essential minichromosome in a *rad3Δ* background (our unpublished results).

We identified isochromosome formation as the predominant mechanism of break-induced extensive LOH in arg^+ $G418^S$ ade^- his^- colonies associated with failed HR repair, resulting in a chromosomal element of 388 kb (35). Analysis of 18 arg^+ $G418^S$ ade^- his^- colonies from a *rad3Δ* background indicated that the majority (78%) were of an identical size to that of a previously characterized isochromosome (388 kb; Figure 2A, left panel, compare lanes 2–4). The remaining four *rad3Δ* arg^+ $G418^S$ ade^- his^- colonies displayed a truncated minichromosome of a smaller size to those corresponding to isochromosomes (Figure 2A, left panel, lane 5). Southern blot analysis, using a probe derived from *Spcc4b3.18*, which anneals directly distal to the centromere on the right arm of Ch^{16}-RMGAH and ChIII (Figure 2A, right panel), showed annealing to the parental minichromosome, but failed to anneal to the chromosomal elements associated with extensive LOH, indicating that these smaller chromosomal elements had lost the entire broken chromosome arm (Figure 2A, right panel).

CGH analysis of an arg^+ $G418^S$ ade^- his^- strain carrying a smaller non-isochromosomal element and a parental strain carrying Ch^{16}-RMGAH showed reduced Log2 hybridization ratios across the right arm of the minichromosome, thus confirming the absence of the right arm of the minichromosome in these LOH colonies (Figure 2B). CGH analysis also failed to show increased ratios across the intact left arm of the minichromosome, indicating that in contrast to the previously characterized isochromosomes, this region had not been duplicated in these less frequent and shorter chromosomal elements and were therefore not isochromosomes (Figure 2B and C; (35)). These findings support a model in which failed HR repair results in extensive end processing leading to Ch^{16} loss or extensive LOH through the formation of isochromosomes or smaller chromosomal elements in a *rad3Δ* background. These less frequently occurring shorter chromosomal elements are likely to have arisen from *de novo* telomere addition at or near the centromere of the minichromosome.

Using a wild-type strain carrying Ch^{16}-MGH, which in contrast to Ch^{16}-RMYAH contains an *ade6-M216* heteroallele, ∼30 kb centromere-proximal to the break site, we have previously identified LOH events resulting in retention of the *ade6-M216* heteroallele, while losing a $G418^R$ marker adjacent to the break site and a *his3* gene ∼30 kb distal to the break site (Supplementary Figure S3A) (39). These LOH events were associated with DSB repair by HR, and included break-induced replication (BIR) and allelic crossovers (39). However, isochromosome formation (in which the entire broken arm is lost) cannot be detected in this assay. Using this Ch^{16}-MGH based assay, no increase in LOH events associated with DSB repair (and retention of the *ade6-M216* heteroallele) was observed in a *rad3Δ* background (Supplementary Figure S3B and C). This contrasts with a role for $Rad3^{ATR}$ in suppressing break-induced LOH

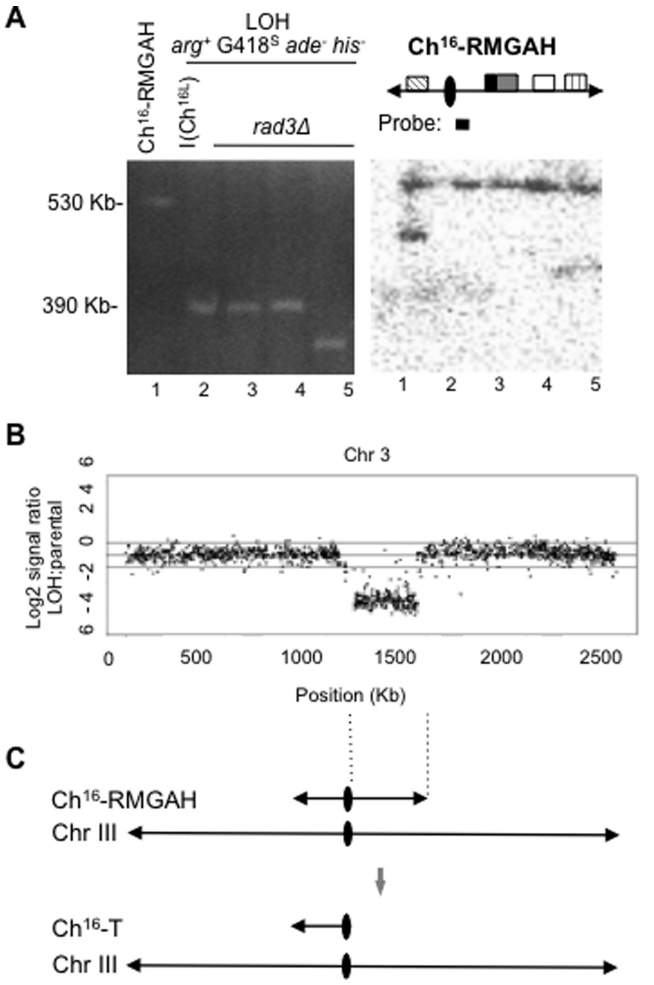

Figure 2. Break-induced extensive LOH in *rad3Δ* results from extensive resection, and predominantly isochromosome formation (**A**). Left panel: PFGE analysis from *rad3Δ* Ch^{16}-RMGAH parental strain (TH2941; lane 1), individual arg^{+} G418^{S} ade^{-} his^{-} (LOH) colonies from wild-type (a CGH confirmed isochromosome I(Ch^{16L}); lane 2) and *rad3Δ* (lanes 3–5) backgrounds following DSB induction are shown. Right panel: Southern blot analysis of the PFGE, probed with Spcc4b3.18, which anneals directly distal the centromere on Ch^{16}-RMGAH and ChIII (as indicated) (**B**). CGH of wild-type Ch^{16}-RMGAH (TH2125) and an arg^{+} G418^{S} ade^{-} his^{-} (LOH) strain (TH8399) carrying a truncated minichromosome that is shorter than the known isochromosome (TH4313) (Figure 2A, lane 1) previously characterized by CGH (35). The Log2 of the LOH:parental signal ratio across the and chromosome III (from which the minichromosome is derived) is shown. **(C)** A schematic of the structure of the smaller chromosomal element arising following DSB induction in a *rad3Δ* background as related to the CGH data. CGH analysis of an isochromosome with a duplicated left arm is presented in Supplementary Figure S2 for comparison.

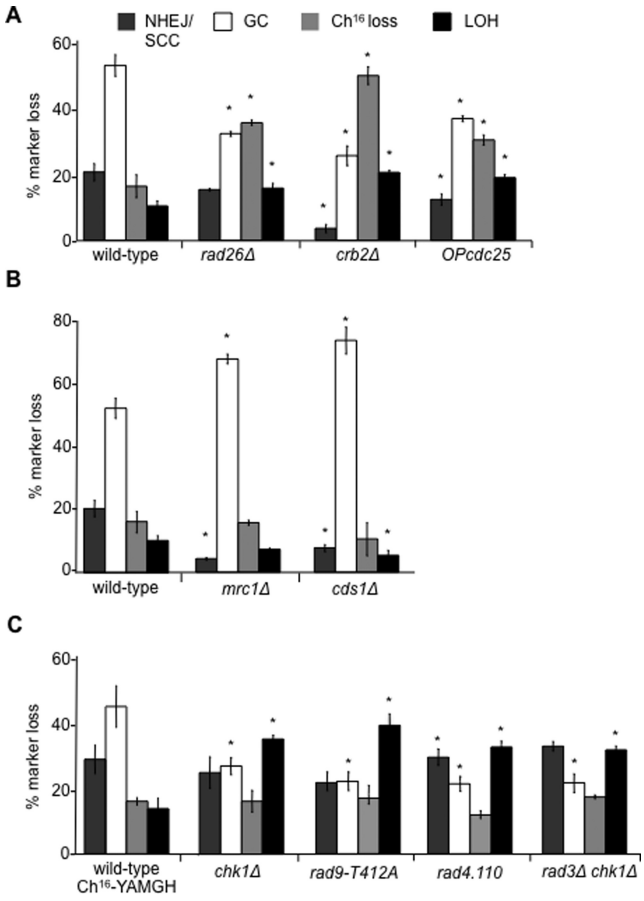

Figure 3. The DNA damage checkpoint promotes HR and suppresses break-induced LOH. (**A**) Percentage DSB-induced marker loss of Ch^{16}-RMGAH in wild-type (TH2130), *rad26Δ* (TH3410), *crb2Δ* (TH3383) and *OPcdc25* (TH3395) backgrounds. (**B**) The DNA replication checkpoint does not suppress break-induced LOH. Percentage DSB-induced marker loss of Ch^{16}-RMGAH in wild-type (TH2130), *mrc1Δ* (TH3253) and *cds1Δ* (TH3256) backgrounds. (**C**) An additional role for Chk1 activation in promoting HR and suppressing break-induced LOH. Percentage DSB-induced marker loss of Ch^{16}-YAMGH in wild-type (TH3317), *chk1Δ* (TH3153), *rad9-T412A* (TH5381), *rad4.110* (TH4481) and *rad3Δchk1Δ* (TH3623) backgrounds. For (A), (B) and (C) the levels of NHEJ/SCC, GC, Ch^{16} loss and extensive LOH are shown. Data are the mean of three experiments and standard errors of the mean are indicated. The asterisk (*) represents $P < 0.05$ compared to wild-type.

leading to isochromosome formation, and further supports a role for Rad3^{ATR} in suppressing extensive LOH associated with failed HR repair.

The DNA damage checkpoint pathway promotes HR and suppresses break-induced LOH and minichromosome loss

To test a general role of the DNA damage checkpoint pathway in suppressing break-induced LOH, levels of marker loss were additionally examined in other checkpoint-deficient strains. Like loss of Rad3^{ATR}, loss of the checkpoint sensor Rad26^{ATRIP}, the checkpoint adaptor Crb2^{53BP1} or overexpression of Cdc25 (*OPcdc25*) led to reduced HR repair, and increased levels of Ch^{16} loss and LOH. In a *rad26Δ* background, GC was significantly reduced (32.7% $P = 0.01$), while levels of Ch^{16} loss (35.6% $P = 0.01$) and break-induced LOH (15.8% $P = 0.05$) were significantly increased, compared to wild-type (Figure 3A). Similarly, in a *crb2Δ* background break-induced NHEJ/SCC (3.6% $P < 0.01$) and GC (25.6% $P < 0.01$) were significantly reduced while Ch^{16} loss (49.8% $P < 0.01$) and LOH (20.5% $P < 0.01$) were significantly increased compared to wild-type (Figure 3A). *OPcdc25* encodes *cdc25* under the control of the strong constitutive *adh* promoter, leading to its overproduction and subsequently to checkpoint loss (26). DSB induction in an *OPcdc25* background resulted in significantly reduced NHEJ/SCC (12.4% $P = 0.03$), significantly

reduced GC (36.8% $P = 0.03$), and significantly increased Ch^{16} loss (30.4% $P = 0.02$) and break-induced LOH (18.9%; $P < 0.01$) compared to wild-type (Figure 3A). Further analysis of at least 16 of the arg^+ $G418^S$ ade^- his^- colonies from the *rad26Δ*, *crb2Δ* or *OPcdc25* backgrounds indicated that they carried a truncated minichromosome of an identical size to that of a known isochromosome (388 kb) (our unpublished results). These findings support a general role for the DNA damage checkpoint pathway in facilitating efficient HR repair and suppressing break-induced chromosomal rearrangements and LOH.

The DNA replication checkpoint does not suppress break-induced LOH

A possible role for the DNA replication checkpoint in DSB repair was also analysed in *mrc1Δ* or *cds1Δ* backgrounds. In contrast to the DNA damage checkpoint mutants, levels of GC were significantly increased in *mrc1Δ* (69.3%; $P < 0.01$), while levels of NHEJ/SCC (4.4%; $P = 0.01$) were significantly reduced compared to wild-type (Figure 3B). Similarly, levels of GC were significantly increased in *cds1Δ* (75.3%; $P < 0.01$), while levels of NHEJ/SCC (7.9%; $P = 0.01$) and LOH (5.4%; $P < 0.01$) were reduced compared to wild-type (Figure 3B). Thus, in contrast to the DNA damage checkpoint pathway, disrupting the DNA replication checkpoint resulted in a hyper-recombinant phenotype.

$Chk1^+$ activation is required to suppress break-induced LOH

To test the role of the DNA damage checkpoint effector kinase Chk1 in suppressing break-induced LOH, the *chk1::ura4* mutant background was established using Ch^{16}-YAMGH in which the *chk1*$^+$ gene present on the minichromosome was deleted with a hygromycin resistance marker. While NHEJ/SCC levels in *chk1Δ* (24.1%) were similar to wild-type Ch^{16}-YAMGH (27.8%), levels of GC were significantly reduced in a *chk1Δ* background (26.0% $P < 0.01$), compared to wild-type Ch^{16}-YAMGH (43.3%). However, levels of break-induced LOH (33.9%) were significantly increased in *chk1Δ* compared to wild-type Ch^{16}-YAMGH (13.3% $P < 0.01$) and *rad3Δ* (19.6% $P < 0.01$) backgrounds, thus suggesting an additional role for Chk1 in suppressing break-induced LOH, to that of $Rad3^{ATR}$. The further increase in levels of break-induced LOH in the *chk1Δ* background was associated with reduced levels of Ch^{16} loss (15.7%), but this was not significantly different to wild-type Ch^{16}-YAMGH (16.3% $P = 0.9$) (Figure 3C). Further PFGE analysis of the *chk1Δ* Hyg^R ade^- $G418^S$ his^- colonies indicated that LOH had resulted from isochromosome formation (our unpublished results).

Chk1 activation requires Rad9 phosphorylation on T412/S423 to promote association with $Rad4^{TOPBP1}$ (17). Therefore, we tested levels of break-induced LOH in *rad9-T412A* and *rad4-110* mutant backgrounds in which Chk1 activation is abrogated. Both resembled the DSB profile of *chk1Δ* with increased break-induced LOH. DSB induction in a *rad9-T412A* background resulted in significantly reduced GC (21.5% $P = 0.01$) and significantly increased break-induced LOH (39.8% $P = 0.02$) compared to wild-type (Figure 3C). Similarly, DSB induction in a *rad4-110* temperature-sensitive background at the semi-permissive temperature of 30°C resulted in significantly elevated levels of NHEJ/SCC (34.5% $P = 0.03$), significantly reduced GC (20.8% GC $P < 0.01$) and significantly increased LOH (32.8% $P < 0.01$) compared to wild-type (Figure 3C).

These results support a role for Chk1 activation in suppressing break-induced LOH, which is functionally distinct from $Rad3^{ATR}$. DSB repair in a *rad3Δchk1Δ* double mutant exhibited a similar DSB repair profile to the *chk1Δ* single mutant (Figure 3C). These findings indicate $Rad3^{ATR}$ and Chk1 function in the same pathway to suppress break-induced LOH and to facilitate efficient Ch^{16} loss. However, Chk1 performs an additional $Rad3^{ATR}$ -independent role in suppressing break-induced LOH.

A distinct role for Rad17 and the 9-1-1 complex in suppressing break-induced LOH

Another component of the DNA damage checkpoint is Rad17 that functions as part of the RFC-checkpoint loading complex to load the 9-1-1 complex onto sites of damaged DNA (13,14). Mutant *loh6-1*, isolated from the screen, was found to encode a nonsense (W72X) mutation in the *rad17*$^+$ gene (Supplementary Figure S4; our unpublished results). DSB induction in a *rad17Δ* background resulted in a striking DSB repair profile, which suggested a distinct role for Rad17 in facilitating extensive resection leading to Ch^{16} loss and suppressing break-induced LOH compared to $Rad3^{ATR}$. *rad17Δ* had significantly reduced levels of GC (34.4% $P = 0.03$) and Ch^{16} loss (0.8%, $P < 0.01$) and significantly increased levels of break-induced LOH (59.1% $P = 0.03$) compared to wild-type (Figure 4A).

The DSB repair profiles of *rad9Δ, rad1Δ* and *hus1Δ* mutants were also examined, and were found to be very similar to those observed for *rad17Δ*: GC was significantly reduced in *rad9Δ* (34.7% $P < 0.01$), *rad1Δ* (41.1% $P < 0.01$) and *hus1Δ* (38.1% $P = 0.01$) backgrounds compared to wild-type (69.6%). Ch^{16} loss was also significantly reduced in *rad9Δ* (1.0% $P < 0.01$), *rad1Δ* (0.19% $P < 0.01$) and *hus1Δ* (1.4% $P < 0.01$) backgrounds compared to wild-type (16.5%). In contrast, break-induced LOH was dramatically and significantly increased in *rad9Δ* (57.4% $P < 0.01$), *rad1Δ* (54.8% $P = 0.01$) and *hus1Δ* (56.8% $P < 0.01$) backgrounds compared to wild-type (9.6%) (Figure 4A).

PFGE analysis of individual LOH colonies (arg^+ $G418^S$/Hyg^S ade^- his^-) derived from each of the *rad17Δ, rad9Δ, rad1Δ* or *hus1Δ* mutant backgrounds confirmed the majority to have a chromosomal element of equivalent size to a known isochromosome. Additionally, shorter chromosomal elements as described earlier were observed in 5 out of 19 (26%) *rad17Δ* LOH colonies, 4 out of 20 (20%) of *rad9Δ* LOH colonies, 4 out of 19 (21%) of *rad1Δ* LOH colonies and 4 out of 17 (24%) of *hus1Δ* LOH colonies (our unpublished results). CGH analysis of one *rad17Δ* arg^+ $G418^S$ ade^- his^- colony indicated the shorter chromosomal element resulted from loss of the broken minichromosome arm while the intact arm was not duplicated (our unpublished results), thus resembling the shorter truncated chromosomal elements observed in the *rad3Δ* LOH colonies (Figure 2B and C).

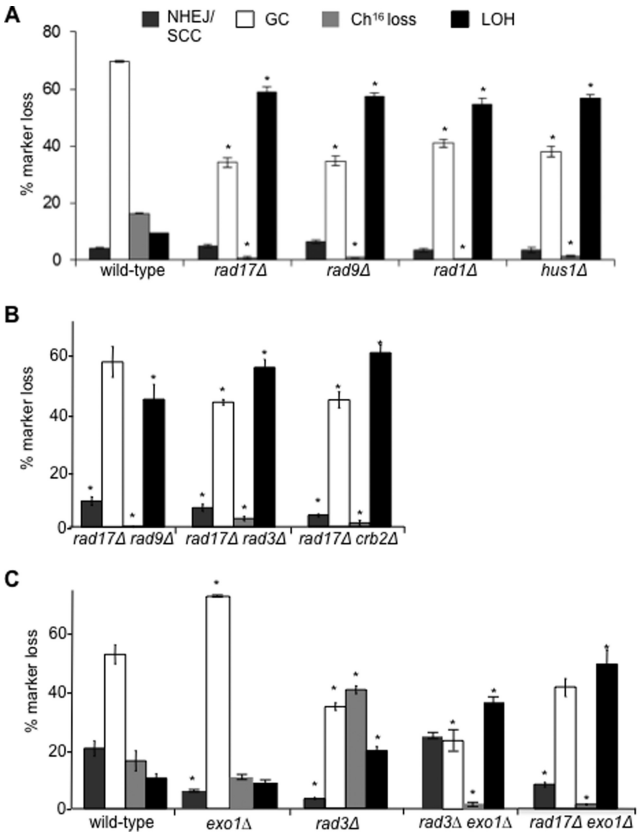

Figure 4. An additional role for Rad17 and the 9-1-1 complex in promoting HR and suppressing break-induced LOH. (**A**) Percentage DSB-induced marker loss of Ch^{16}-RMYAH in wild-type (TH4104, TH4121, TH4122, TH4125), *rad17Δ* (TH7427-TH7430), *rad9Δ* (TH7588-TH7591), *rad1Δ* (TH7493, TH7494, TH7495) and *hus1Δ* (TH7431-TH7434) backgrounds. (**B**) Percentage DSB-induced marker loss of Ch^{16}-RMGAH in *rad17Δ rad9Δ* (TH3454), *rad17Δ rad3Δ* (TH3455) and *rad17Δ crb2Δ* (TH3529) backgrounds. (**C**) $Rad3^{ATR}$ and Exo1 function redundantly to suppress break-induced LOH. Percentage DSB-induced marker loss of Ch^{16}-RMGAH in wild-type (TH2130), *exo1Δ* (TH3378), *rad3Δ* (TH2941), *rad3Δexo1Δ* (TH3382) and *rad17Δ exo1Δ* (TH3701) backgrounds. For (A), (B) and (C) the levels of NHEJ/SCC, GC, Ch^{16} loss and extensive LOH are shown. Data are the mean of three experiments and standard errors of the mean are indicated. The asterisk (*) represents significant difference compared to wild-type.

Given the strikingly similar DSB-induced marker loss profiles observed in *rad17Δ, rad9Δ, rad1Δ* and *hus1Δ*, we tested the possibility that they functioned in the same pathway by epistasis analysis. Break-induced marker loss in a *rad17Δrad9Δ* double mutant was very similar to the single mutants, *rad17Δ* and *rad9Δ* (Figure 4B), supporting roles for the Rad17 loading clamp and 9-1-1 complex acting in the same pathway to suppress break-induced LOH. A double mutant *rad17Δrad3Δ* was also constructed. This strain exhibited similar levels of break-induced LOH (50.2%) and levels of Ch^{16} loss (2.7%) to a *rad17Δ* mutant (49.3% and 1.4%, respectively, Figure 4B). Thus Rad17 performs an additional role in extensive resection and suppression of break-induced LOH to that of $Rad3^{ATR}$. As increased levels of break-induced extensive LOH correlated with reduced levels of Ch^{16} loss these findings support a role for Rad17 and the 9-1-1 complex in facilitating extensive end-processing required for Ch^{16} loss. The *S. cerevisiae crb2*$^+$ homologue, *RAD9*, has been shown to limit the amount of ssDNA produced at uncapped telomeres (41). We found *rad17Δcrb2Δ* double mutants exhibited similar levels of SCC (3.5%), GC (39.9%), Ch^{16} loss (1.2%) and break-induced LOH (50.2%) as those observed in a *rad17Δ* single mutant (Figure 4B) . These results suggested that $Crb2^{53BP1}$ was not limiting extensive resection in a *rad17Δ* mutant background in *S. pombe*.

Analysis of spontaneous isochromosome formation within the Ch^{16} minichromosome indicates that they contain the breakpoint in centromere repeats, showing that isochromosomes are produced by centromere rearrangements. $Rad3^{ATR}$ has been previously shown to suppress spontaneous isochromosome formation associated with increased centromeric recombination (42). We therefore tested whether deletion of *rad9*$^+$ exhibited increased spontaneous centromeric recombination. However, deletion of *rad9*$^+$ did not significantly increase the rate of spontaneous recombination between the *ade6B* and *ade6X* heteroalleles integrated into the centromere (Supplementary Figure S5A and B), consistent with the idea that $Rad9^{Sp}$ affects resection of DSB-induced ends, generated outside the centromere.

$Rad3^{ATR}$ and Exo1 act redundantly to suppress break-induced LOH

In *S. cerevisiae*, Mec1 is required for the inhibitory phosphorylation of Exo1 (43). We therefore tested the relationship between $Rad3^{ATR}$ and Exo1. DSB induction in an *exo1Δ* background resulted in significantly reduced levels of NHEJ/SCC (7.6% $P = 0.01$), and significantly elevated levels of GC (69.8% $P = 0.02$) when compared to wild-type (Figure 4C). DSB induction in a *rad3Δ exo1Δ* background resulted in significantly reduced GC in a *rad3Δ exo1Δ* background (28.3% $P < 0.01$) compared to wild-type (52.7%). A dramatic decrease in Ch^{16} loss was observed in the *rad3Δ exo1Δ* double mutant (1.24% $P = 0.02$) in comparison to wild-type (16.3%) *exo1Δ* (11.4% $P < 0.01$) and *rad3Δ* (40.5% $P < 0.01$) single mutants. Importantly, in the *rad3Δexo1Δ* double mutant the level of break-induced LOH was strikingly increased (41.6% $P < 0.01$) compared to wild-type (10.3%; Figure 4C). These data are consistent with the idea that Rad3 phosphorylates Exo1, thus inactivating it. PFGE analysis of the arg^+ $G418^S$ ade^- his^- colonies derived from the *rad3Δ exo1Δ* mutant background confirmed that LOH had arisen predominantly through isochromosome formation, with smaller chromosomal elements observed in 3/17 (18%) of the individually isolated LOH colonies examined (our unpublished results). This contrasts with the finding that the *rad17Δexo1Δ* double mutant did not affect the levels of break-induced LOH compared to *rad17Δ* (Figure 4C).

Deleting *spd1*$^+$ suppresses HR defects of *rad3Δ,rad26Δ* but not 9-1-1 mutants

We previously identified a role for $Rad3^{ATR}$ in facilitating efficient HR repair by inducing nucleotide synthesis

in response to DSBs. This allows efficient DNA synthesis during HR, preventing LOH. Rad3^{ATR} induces Ddb1-Cul4^{Cdt2} ubiquitin ligase dependent degradation of the ribonucleotide reductase (RNR) inhibitor Spd1 to increase nucleotide pools (44). Transactivation of Cdt2 is required for the recruitment of Spd1 to the Ddb1-Cul4^{Cdt2} complex and requires Rad3^{ATR} and Chk1 (45).

Given the contrasting repair profiles of *rad3Δ* and *rad9Δ*, *rad1Δ* or *hus1Δ* deletion strains, we investigated the role of the 9-1-1 complex in Cdt2 accumulation and thus dNTP synthesis. Deletion of *rad3*$^+$, *rad26*$^+$, *rad17*$^+$, *rad9*$^+$, *rad1*$^+$ and *hus1*$^+$ each abolished nuclear accumulation of Cdt2 in response to DNA damage (Supplementary Figure S6A and B). These findings are consistent with a common role for the DNA damage checkpoint pathway in facilitating dNTP synthesis through Cdt2 transactivation.

To further test the role of DNA damage checkpoint genes in dNTP synthesis, we tested whether deleting *spd1*$^+$, an inhibitor of ribonucleotide reductase (46), might suppress the DNA damage sensitivity of other checkpoint mutants by increasing cellular nucleotide pools. We found that deletion of *spd1*$^+$ could partially suppress the bleocin sensitivity of *rad3Δ* and *rad26Δ* (Figure 5A). In contrast, deletion of *spd1*$^+$ was unable to suppress the bleocin sensitivity of *rad17Δ, rad9Δ, rad1Δ* or *hus1Δ* (Figure 5A).

To confirm that suppression of bleocin sensitivity by *spd1Δ* correlated with increased HR, DSB assays were performed on these strains. Consistent with this, DSB induction in a *rad26Δ spd1Δ* background resulted in significantly increased levels of GC (32.4%, $P = 0.02$) and significantly reduced levels of LOH (23.4%, $P = 0.02$), compared to *rad26Δ* (GC 15.6%; LOH 36.3%, respectively) (Figure 5B), as was previously observed for *rad3Δ spd1Δ* (44). These findings are consistent with roles for both Rad3^{ATR} and Rad26^{ATRIP} in facilitating efficient HR by promoting nucleotide synthesis. In contrast, deletion of *spd1*$^+$ in *rad17Δ, rad9Δ, rad1Δ* or *hus1Δ* backgrounds did not result in suppression of HR or a reduction in LOH compared to the parental strains following DSB induction (Figure 5C and our unpublished results). Together these results indicate a role for Rad3^{ATR} Rad26^{ATRIP}, Rad17 and the 9-1-1 complex in DNA damage induced dNTP synthesis, while Rad17 and the 9-1-1 complex also perform an additional function from that of Rad3^{ATR} Rad26^{ATRIP} that cannot be suppressed by *spd1*$^+$ deletion.

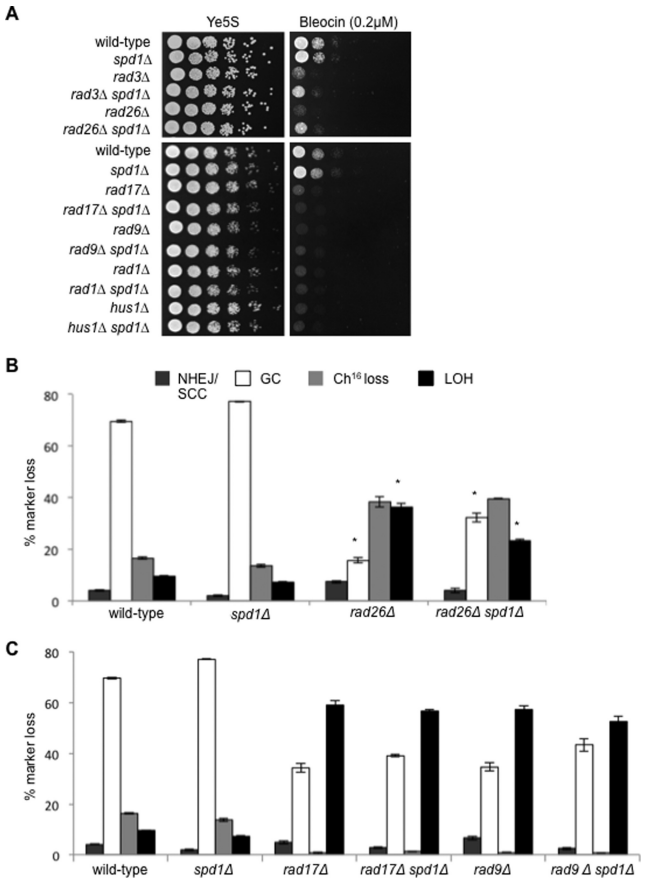

Figure 5. *spd1Δ* suppresses the repair defect of *rad3Δ* and *rad26Δ*. (**A**) Five-fold serial dilutions of wild-type (TH2094), *spd1Δ* (TH4355), *rad3Δ* (TH7329), *rad3Δspd1Δ* (TH8295), *rad26Δ* (TH7330) and *rad26Δspd1Δ* (TH8194) strains (top panel) and wild-type (TH2094), *spd1Δ* (TH4355), *rad17Δ* (TH7331), *rad17Δspd1Δ* (TH7794), *rad9Δ* (TH7414), *rad9Δspd1Δ* (TH7146), *rad1Δ* (TH7333), *rad1Δspd1Δ* (TH8249), *hus1Δ* (TH8296) and *hus1Δspd1Δ* (TH8195) strains (bottom panel) grown on Ye5S (untreated) and Ye5S + 0.2 μg/ml bleocin. (**B**) Percentage DSB-induced marker loss in wild-type (TH4121, TH4122, TH4104), *spd1Δ* (TH4077-TH4079) *rad26Δ* (TH7424-TH7426) and *rad26Δspd1Δ* (TH7585-TH7587) backgrounds. Means ± standard errors of three experiments are shown. Asterisk (*) represents significant difference compared to *rad26Δ* and *rad26Δspd1Δ* mutants. (**C**) Percentage DSB-induced marker loss in wild-type (TH4121, TH4122, TH4104), *spd1Δ* (TH4077-TH4079), *rad17Δ* (TH7429-TH7430), *rad17Δspd1Δ* (TH7566-TH7568), *rad9Δ* (TH7589-TH7591) and *rad9Δspd1Δ* (TH7464-TH7466) backgrounds. Means ± standard errors of three experiments are shown.

Role for Rad17 and the 9-1-1 complex in facilitating DSB end resection and SSA

To further test a role for the 9-1-1 complex in DSB resection, we utilized a strain in which DSB-induced extensive resection facilitates SSA of two overlapping regions of the *LEU2* gene containing sequence homology, placed either side of a break site (Figure 6A). The HO endonuclease was placed under the control of the endogenous *urg* promoter, which is rapidly inducible with uracil, generating a unique DSB at the HO cut site (HO-cs) (37,38). DSB induction in wild-type *rad3Δ, rad17Δ* and *rad9Δ* backgrounds was observed genetically by loss of histidine auxotrophy and found to be comparable between the mutants (Figure 6B). The repair kinetics was next determined by Southern blot analysis of the levels of loss of a 6.2 kb band and the appearance of a shorter 3.1 kb band containing the reformed *LEU2* gene resulting from SSA (Figure 6A). In a wild-type or *rad3Δ* background DSB induction resulted in almost complete loss of the upper 6.2 kb band, and generation of a much stronger 3.1 kb band after 360 min, consistent with efficient extensive resection and SSA repair (Figure 6C and D). In contrast, DSB induction in a *rad17Δ* or *rad9Δ* background resulted in formation of a weaker 3.1 kb band consistent with reduced extensive resection and SSA repair in these backgrounds (Figure 6C and D). These findings support roles for Rad17 and the 9-1-1 complex in extensive resection and SSA repair.

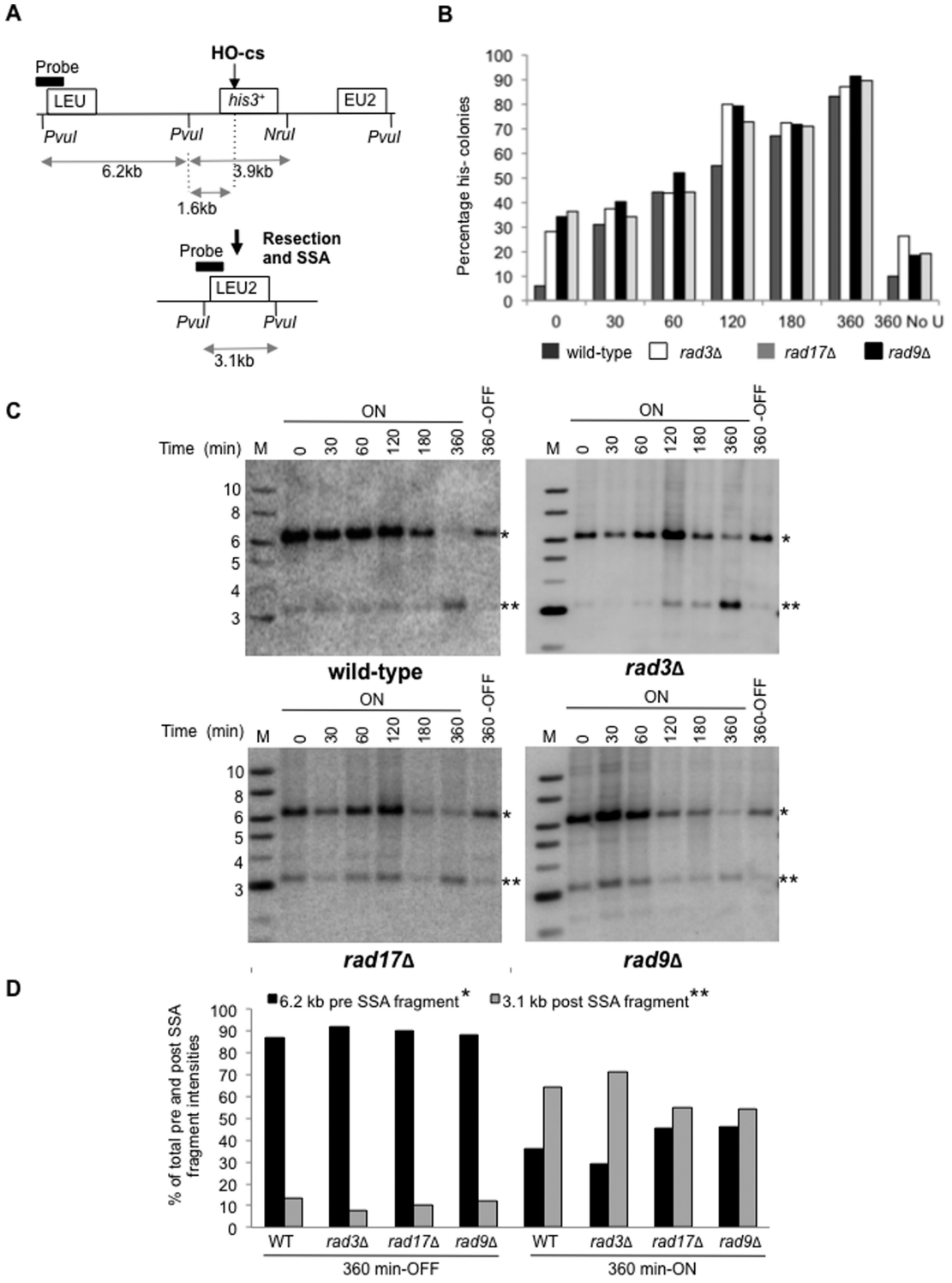

Figure 6. A role for Rad17 and the 9-1-1 complex in SSA repair. (**A**) A schematic of a resection and SSA assay as previously described (37). (**B**) Graph of HOcs-HIS SSA genetic colony assay showing loss of his3+ marker following induction of Purg1lox-HO-endonuclease in wild-type (TH7184), *rad3Δ* (TH8091) *rad17Δ* (TH8040) and *rad9Δ* (TH8050) backgrounds. The genetic assay was repeated independently at least three times. Error bars are ± standard deviation of the mean. (**C**) Physical analysis of HO-endonuclease cutting and repair by Southern hybridization in wild-type (TH7184), *rad3Δ* (TH8091) *rad17Δ* (TH8040) and *rad9Δ*(TH8050) cells. Genomic DNA extracted after Purg1lox induction at intervals shown, digested with PvuI and NruI, blotted and hybridized to probe as indicated in (A). Marker lane (M) and band sizes (kb) are indicated. The 6.2 kb pre-SSA fragment (*) and 3.1 kb post-SSA fragment (**) are indicated. (**D**) Graph of band intensities at 360 min without HO induction (OFF) or with HO induction (ON) for blots shown in (C). Blots were scanned using a personal molecular imager^{TM} (PMITM) and Quantity One Software (Bio-rad). Relative intensities of 6.2 kb pre-SSA fragment and 3.1 kb post-SSA fragments are shown, and were normalized by calculating the intensities of pre- and post-SSA bands as a percentage of the total intensities for these bands for each time point. M indicates DNA size marker and kb sizes of marker bands shown. 360 OFF refers to cells grown in EMM+L+H.

DISCUSSION

Here we establish roles for the DNA damage checkpoint pathway in facilitating efficient HR, and suppressing break-induced chromosomal rearrangements associated with failed HR repair. We define distinct yet overlapping functions for the DNA damage checkpoint genes in facilitating both extensive resection and nucleotide synthesis thereby promoting HR repair. These findings suggest that the DNA damage checkpoint pathway plays an important role in coordinating these processes in addition to promoting cell cycle arrest in response to DSBs.

A common role for the DNA damage checkpoint pathway was identified in facilitating nucleotide synthesis in response to DNA damage. Consistent with this, we found *rad3*$^+$, *rad26*$^+$, *rad17*$^+$, *rad9*$^+$, *rad1*$^+$ and *hus1*$^+$ genes to be required for transactivating Cdt2 expression in response to DNA damage. Checkpoint activation has previously been shown to lead to Cdt2 transactivation, which in turn activates the Ddb1-Cul4^{Cdt2} ubiquitin ligase complex leading to degradation of Spd1, an RNR inhibitor in fission yeast (45). The resulting increase in nucleotide synthesis following RNR activation has been shown to promote HR repair by facilitating gap filling of resected ssDNA ends (44). Accordingly, we found increased nucleotide synthesis resulting from *spd1*$^+$ deletion could partially suppress the DNA damage sensitivity and HR deficiency of *rad26Δ*, as well as that of *rad3Δ,* as previously described (44). However, *spd1*$^+$ deletion was unable to suppress the DNA damage sensitivity and HR deficiency of *rad17Δ rad9Δ*, *rad1Δ* or *hus1Δ*, consistent with an additional role for Rad17 and the 9-1-1 complex in the DNA damage response.

An additional role for Rad17 and the 9-1-1 complex in extensive resection was identified. Deletion of *rad17*$^+$ *rad9*$^+$, *rad1*$^+$ and *hus1*$^+$ genes resulted in a remarkable reduction in break-induced Ch^{16} loss and a concomitant increase in chromosomal rearrangements, predominantly through isochromosome formation. Given that Ch^{16} loss was previously shown to arise from extensive resection from the break site (35), these findings suggest roles for the Rad17 and the 9-1-1 complex in facilitating efficient resection through centromeric DNA (Figure 7A). Further, using a physical assay, we confirmed a role for Rad17 and the 9-1-1 complex in resection and SSA repair, strongly supporting the genetic data for the 9-1-1 complex in facilitating extensive resection. Moreover, *rad17Δ* functioned epistatically with *rad9Δ*, consistent with a role for Rad17 in loading the 9-1-1 complex (18). As no increase in spontaneous centromere recombination was observed in a *rad9Δ* background compared to wild-type, these findings further support a role for Rad17 and the 9-1-1 complex in DSB metabolism. Consistent with these findings, roles for homologues of Rad17 and the 9-1-1 complex in DSB resection have been reported previously (41,47–49).

Isochromosomes were previously determined to have arisen from extensive resection resulting from failed HR leading to BIR within the centromere, and to duplication of the intact minichromosome arm (35). We speculate that the striking increase in break-induced isochromosomes and reduced chromosome loss observed in the absence of Rad17 or the 9-1-1 complex may reflect the increased stability of

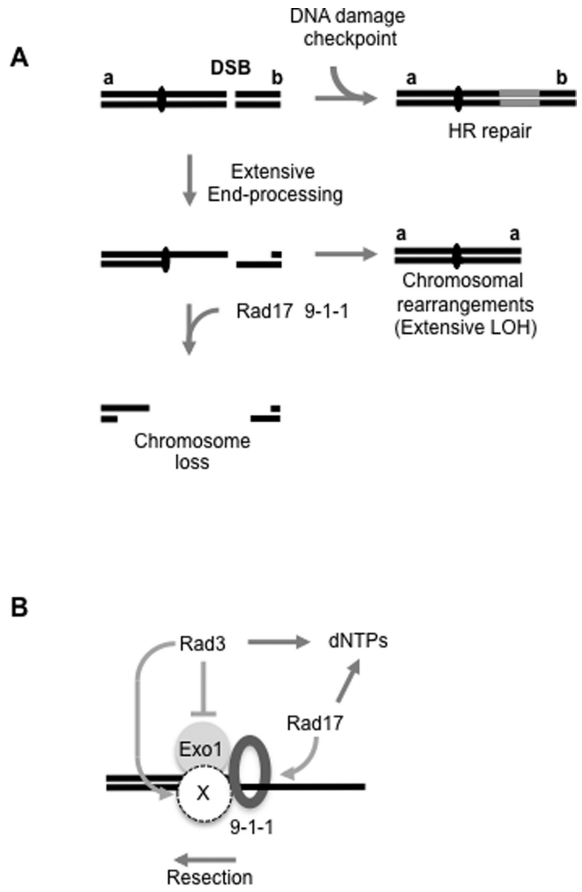

Figure 7. (**A**) Model for roles for the DNA damage checkpoint pathway in suppressing extensive LOH and chromosomal rearrangements associated with failed DSB repair. The DNA damage checkpoint pathway promotes efficient HR repair. Failed HR leads to extensive end processing and to chromosome loss or rearrangements. Rad17 and the 9-1-1 complex further suppress break-induced LOH by promoting extensive end processing through the centromere, resulting in loss of the broken chromosome. This is supported by the findings that Rad17 and the 9-1-1 complex are required for extensive resection, removal of the unrepaired broken minichromosome and suppression of extensive LOH. (**B**) Model for the roles of the DNA damage checkpoint proteins and Exo1 in facilitating extensive resection in *S. pombe.* Following DSB induction, the 9-1-1 complex (ring) is loaded by Rad17. The 9-1-1 complex facilitates processivity of Exo1 and nuclease X. Rad3^{ATR}, together with other checkpoint proteins (not shown), promotes dNTP synthesis, promotes nuclease X and additionally inhibits Exo1. This model is supported by the findings that the *rad3Δ exo1Δ* double mutant phenocopies the DSB repair profile of *rad17Δ,* leading to high levels of extensive LOH and low levels of minichromosome loss, while *rad3Δ* or *exo1Δ* do not; as *exo1Δ* was not equivalent to *rad17Δ* or loss of the 9-1-1 complex, this suggests that the 9-1-1 complex additionally provides processivity to another nuclease (X), which requires Rad3 for activity. All checkpoint genes tested are required for transactivating Cdt2 expression, an initial step in damage-induced dNTP synthesis. See the text for details.

DSB repair intermediates arising through reduced resection efficiency, thereby facilitating BIR. Together these findings underline the importance of efficient DSB resection in maintaining genome stability.

We further identified deletions of *rad3*$^+$ or *exo1*$^+$ to be epistatic with deletion of *rad17*$^+$ suggesting that Rad3, Exo1, Rad17 and the 9-1-1 complex function in the same pathway to facilitate extensive resection and Ch^{16} loss. In contrast to the single mutants, simultaneous deletion of

rad3^{+} and *exo1*$^{+}$ was found to be functionally equivalent to deletion of *rad17*$^{+}$, resulting in very high levels of break-induced LOH and low levels of Ch^{16} loss. These findings suggest a role for Rad3^{ATR} in inhibiting Exo1 activity, consistent with findings in *S. cerevisiae* (43). Thus in the absence of Rad3, reduced GC leads to increased levels of Exo1-dependent resection resulting in increased levels of Ch^{16} loss and LOH. However, in the absence of both Rad3 and Exo1, extensive resection becomes inefficient, resulting in reduced Ch^{16} loss and very high levels of LOH. As the repair profile of the *rad3Δ exo1Δ* double mutant is similar to those observed in *rad17Δ, rad9Δ, rad1Δ* or *hus1Δ* backgrounds, these findings suggest the 9-1-1 complex functions to promote efficient resection through supporting Exo1 activity. In this respect, the 9-1-1 complex may function analogously to structurally related PCNA to provide processivity to Exo1. That the phenotype associated with loss of Exo1 was not equivalent to the loss of Rad17 or the 9-1-1 complex strongly suggests that the 9-1-1 complex additionally provides processivity to another nuclease (X) that acts redundantly with Exo1 to promote extensive resection (Figure 7B). As *rad3Δ exo1Δ* exhibits a phenotype equivalent to *rad17Δ* while *exo1Δ* does not suggest that Rad3^{ATR} may additionally promote nuclease X activity, which is also facilitated by the 9-1-1 complex. A likely candidate for nuclease X is Dna2, which is required for extensive resection, functions in a parallel pathway to Exo1 (50,51), and can be targeted by Rad3^{ATR}, albeit through Cds1^{Chk2} (52).

Our data further identified a distinct role for Chk1 activation in facilitating HR and suppressing break-induced chromosomal rearrangements. As Chk1 activation requires Rad3^{ATR}-dependent phosphorylation, and Rad3^{ATR} activation requires the Rad17 and the 9-1-1 complex (reviewed in (53)), these data suggest that Rad17-dependent loading of the 9-1-1 complex may facilitate Rad3^{ATR} activation and thus Chk1 activation. Yet, we previously found that in contrast to *rad3Δ* the DNA damage sensitivity of *chk1Δ* could not be suppressed by *spd1Δ* (44). Chk1 may therefore function like the 9-1-1 complex to support both Rad3^{ATR}- and Exo1-dependent extensive resection. However, *rad17Δ* and *chk1Δ* backgrounds exhibit distinct DSB repair profiles suggesting that the relationship between these checkpoint proteins is more complex.

In contrast to the DNA damage checkpoint genes, deletion of the replication checkpoint genes *mrc1*$^{+}$ and *cds1*$^{+}$ resulted in a hyper-recombinant phenotype, exhibiting significantly elevated levels of break-induced GC compared to wild-type. These findings indicate a clear demarcation of the DNA damage and replication checkpoint functions, with the former facilitating efficient DSB repair by HR. One possible explanation for this 'hyper-rec' phenotype associated with the replication checkpoint mutants is a role for Mrc1 in promoting sister chromatid cohesion in *S. cerevisiae* (54). As sister chromatid cohesion limits recombination between homologous chromosomes (55), disrupting sister chromatid cohesion through such mutations could facilitate increased levels of interchromosomal GC.

We have identified roles for the DNA damage checkpoint pathway, including homologues of the haploinsufficient tumor suppressors, Rad3^{ATR}, Crb2^{53BP1} and Chk1 in suppressing break-induced LOH (56–58). Our data suggest that these homologues may function to suppress tumorigenesis through promoting efficient HR thereby suppressing extensive resection, chromosomal rearrangements and extensive LOH. In addition, we found that overexpression of Cdc25, which abrogates the DNA damage checkpoint, resulted in inefficient HR repair, increased levels of break-induced chromosome loss and LOH. Reduced HR efficiency following Cdc25 overexpression may have arisen from inappropriate cyclin-dependent kinase (CDK) dependent activation of CtIP and thus extensive resection, as suggested from studies in *S. cerevisiae* (59), or alternatively through a reduced G2-phase and accelerated entry into mitosis through increased CDK activity. In humans, CDC25 orthologues can function as oncogenes and are frequently over expressed in high-grade tumours with poor prognosis (reviewed in (60)). Our findings suggest a mechanistic explanation for these observations.

SUPPLEMENTARY DATA

Supplementary Data are available at NAR Online.

ACKNOWLEDGEMENT

We thank the laboratory of Antony Carr for strains and reagents.

FUNDING

Medical Research Council [R06538 to H.T.P., E.B., T.K., L.H., S.H., R.D., C.W., C.P., T.H.]; Cancer Research UK [C9546/A6517 to S.M., J.B.]; A*STAR, Singapore (to B.W.); Grant-in-Aid for Scientific Research from the Japan Society for the Promotion of Science (to T.N.). Source of open access funding: MRC (T.H.).
Conflict of interest. None declared.

REFERENCES

1. Kasparek,T.R. and Humphrey,T.C. (2011) DNA double-strand break repair pathways, chromosomal rearrangements and cancer. *Semin. Cell Dev. Biol.*, **22**, 886–897.
2. Weinert,T.A. and Hartwell,L.H. (1988) The RAD9 gene controls the cell cycle response to DNA damage in *Saccharomyces cerevisiae*. *Science*, **241**, 317–322.
3. Bashkirov,V.I., Bashkirova,E.V., Haghnazari,E. and Heyer,W.D. (2003) Direct kinase-to-kinase signaling mediated by the FHA phosphoprotein recognition domain of the Dun1 DNA damage checkpoint kinase. *Mol. Cell. Biol.*, **23**, 1441–1452.
4. Zhao,X., Muller,E.G. and Rothstein,R. (1998) A suppressor of two essential checkpoint genes identifies a novel protein that negatively affects dNTP pools. *Mol. Cell*, **2**, 329–340.
5. Bashkirov,V.I., King,J.S., Bashkirova,E.V., Schmuckli-Maurer,J. and Heyer,W.D. (2000) DNA repair protein Rad55 is a terminal substrate of the DNA damage checkpoints. *Mol. Cell. Biol.*, **20**, 4393–4404.
6. Martin,S.G., Laroche,T., Suka,N., Grunstein,M. and Gasser,S.M. (1999) Relocalization of telomeric Ku and SIR proteins in response to DNA strand breaks in yeast. *Cell*, **97**, 621–633.
7. Lisby,M., Mortensen,U.H. and Rothstein,R. (2003) Colocalization of multiple DNA double-strand breaks at a single Rad52 repair centre. *Nat. Cell Biol.*, **5**, 572–577.
8. Harper,J.W. and Elledge,S.J. (2007) The DNA damage response: ten years after. *Mol. Cell*, **28**, 739–745.
9. Abraham,R.T. (2001) Cell cycle checkpoint signaling through the ATM and ATR kinases. *Genes Dev.*, **15**, 2177–2196.

10. Ellison,V. and Stillman,B. (2003) Biochemical characterization of DNA damage checkpoint complexes: clamp loader and clamp complexes with specificity for 5' recessed DNA. *PLoS Biol.*, **1**, E33.
11. Green,C.M., Erdjument-Bromage,H., Tempst,P. and Lowndes,N.F. (2000) A novel Rad24 checkpoint protein complex closely related to replication factor C. *Curr. Biol.*, **10**, 39–42.
12. Thelen,M.P., Venclovas,C. and Fidelis,K. (1999) A sliding clamp model for the Rad1 family of cell cycle checkpoint proteins. *Cell*, **96**, 769–770.
13. Majka,J. and Burgers,P.M. (2003) Yeast Rad17/Mec3/Ddc1: a sliding clamp for the DNA damage checkpoint. *Proc. Natl. Acad. Sci. U.S.A.*, **100**, 2249–2254.
14. Bermudez,V.P., Lindsey-Boltz,L.A., Cesare,A.J., Maniwa,Y., Griffith,J.D., Hurwitz,J. and Sancar,A. (2003) Loading of the human 9-1-1 checkpoint complex onto DNA by the checkpoint clamp loader hRad17-replication factor C complex in vitro. *Proc. Natl. Acad. Sci. U.S.A.*, **100**, 1633–1638.
15. Zou,L. and Elledge,S.J. (2003) Sensing DNA damage through ATRIP recognition of RPA-ssDNA complexes. *Science*, **300**, 1542–1548.
16. Bonilla,C.Y., Melo,J.A. and Toczyski,D.P. (2008) Colocalization of sensors is sufficient to activate the DNA damage checkpoint in the absence of damage. *Mol. Cell*, **30**, 267–276.
17. Furuya,K., Poitelea,M., Guo,L., Caspari,T. and Carr,A.M. (2004) Chk1 activation requires Rad9 S/TQ-site phosphorylation to promote association with C-terminal BRCT domains of Rad4TOPBP1. *Genes Dev.*, **18**, 1154–1164.
18. Navadgi-Patil,V.M. and Burgers,P.M. (2009) The unstructured C-terminal tail of the 9-1-1 clamp subunit Ddc1 activates Mec1/ATR via two distinct mechanisms. *Mol. Cell*, **36**, 743–753.
19. Saka,Y., Esashi,F., Matsusaka,T., Mochida,S. and Yanagida,M. (1997) Damage and replication checkpoint control in fission yeast is ensured by interactions of Crb2, a protein with BRCT motif, with Cut5 and Chk1. *Genes Dev.*, **11**, 3387–3400.
20. Alcasabas,A.A., Osborn,A.J., Bachant,J., Hu,F., Werler,P.J., Bousset,K., Furuya,K., Diffley,J.F., Carr,A.M. and Elledge,S.J. (2001) Mrc1 transduces signals of DNA replication stress to activate Rad53. *Nat. Cell Biol.*, **3**, 958–965.
21. Tanaka,K. and Russell,P. (2001) Mrc1 channels the DNA replication arrest signal to checkpoint kinase Cds1. *Nat. Cell Biol.*, **3**, 966–972.
22. Furnari,B., Rhind,N. and Russell,P. (1997) Cdc25 mitotic inducer targeted by chk1 DNA damage checkpoint kinase. *Science*, **277**, 1495–1497.
23. Boddy,M.N., Furnari,B., Mondesert,O. and Russell,P. (1998) Replication checkpoint enforced by kinases Cds1 and Chk1. *Science*, **280**, 909–912.
24. Zeng,Y., Forbes,K.C., Wu,Z., Moreno,S., Piwnica-Worms,H. and Enoch,T. (1998) Replication checkpoint requires phosphorylation of the phosphatase Cdc25 by Cds1 or Chk1. *Nature*, **395**, 507–510.
25. Lopez-Girona,A., Furnari,B., Mondesert,O. and Russell,P. (1999) Nuclear localization of Cdc25 is regulated by DNA damage and a 14–3–3 protein. *Nature*, **397**, 172–175.
26. Enoch,T. and Nurse,P. (1990) Mutation of fission yeast cell cycle control genes abolishes dependence of mitosis on DNA replication. *Cell*, **60**, 665–673.
27. Myung,K., Datta,A. and Kolodner,R.D. (2001) Suppression of spontaneous chromosomal rearrangements by S phase checkpoint functions in *Saccharomyces cerevisiae*. *Cell*, **104**, 397–408.
28. Myung,K., Chen,C. and Kolodner,R.D. (2001) Multiple pathways cooperate in the suppression of genome instability in *Saccharomyces cerevisiae*. *Nature*, **411**, 1073–1076.
29. Myung,K. and Kolodner,R.D. (2003) Induction of genome instability by DNA damage in *Saccharomyces cerevisiae*. *DNA Repair (Amst)*, **2**, 243–258.
30. Myung,K. and Kolodner,R.D. (2002) Suppression of genome instability by redundant S-phase checkpoint pathways in *Saccharomyces cerevisiae*. *Proc. Natl. Acad. Sci. U.S.A.*, **99**, 4500–4507.
31. Admire,A., Shanks,L., Danzl,N., Wang,M., Weier,U., Stevens,W., Hunt,E. and Weinert,T. (2006) Cycles of chromosome instability are associated with a fragile site and are increased by defects in DNA replication and checkpoint controls in yeast. *Genes Dev.*, **20**, 159–173.
32. Callen,E., Jankovic,M., Difilippantonio,S., Daniel,J.A., Chen,H.T., Celeste,A., Pellegrini,M., McBride,K., Wangsa,D., Bredemeyer,A.L. *et al.* (2007) ATM prevents the persistence and propagation of chromosome breaks in lymphocytes. *Cell*, **130**, 63–75.
33. Khanna,K.K., Lavin,M.F., Jackson,S.P. and Mulhern,T.D. (2001) ATM, a central controller of cellular responses to DNA damage. *Cell Death Differ.*, **8**, 1052–1065.
34. Prudden,J., Evans,J.S., Hussey,S.P., Deans,B., O'Neill,P., Thacker,J. and Humphrey,T. (2003) Pathway utilization in response to a site-specific DNA double-strand break in fission yeast. *EMBO J.*, **22**, 1419–1430.
35. Tinline-Purvis,H., Savory,A.P., Cullen,J.K., Dave,A., Moss,J., Bridge,W.L., Marguerat,S., Bahler,J., Ragoussis,J., Mott,R. *et al.* (2009) Failed gene conversion leads to extensive end processing and chromosomal rearrangements in fission yeast. *EMBO J.*, **28**, 3400–3412.
36. Hope,J.C., Mense,S.M., Jalakas,M., Mitsumoto,J. and Freyer,G.A. (2006) Rqh1 blocks recombination between sister chromatids during double strand break repair, independent of its helicase activity. *Proc. Natl. Acad. Sci. U.S.A.*, **103**, 5875–5880.
37. Watt,S., Mata,J., Lopez-Maury,L., Marguerat,S., Burns,G. and Bahler,J. (2008) urg1: a uracil-regulatable promoter system for fission yeast with short induction and repression times. *PLoS One*, **3**, e1428.
38. Watson,A.T., Werler,P. and Carr,A.M. (2011) Regulation of gene expression at the fission yeast *Schizosaccharomyces pombe* urg1 locus. *Gene*, **484**, 75–85.
39. Cullen,J.K., Hussey,S.P., Walker,C., Prudden,J., Wee,B.Y., Dave,A., Findlay,J.S., Savory,A.P. and Humphrey,T.C. (2007) Break-induced loss of heterozygosity in fission yeast: dual roles for homologous recombination in promoting translocations and preventing de novo telomere addition. *Mol. Cell. Biol.*, **27**, 7745–7757.
40. Jiang,X., Sun,Y., Chen,S., Roy,K. and Price,B.D. (2006) The FATC domains of PIKK proteins are functionally equivalent and participate in the Tip60-dependent activation of DNA-PKcs and ATM. *J. Biol. Chem.*, **281**, 15741–15746.
41. Lydall,D. and Weinert,T. (1995) Yeast checkpoint genes in DNA damage processing: implications for repair and arrest. *Science*, **270**, 1488–1491.
42. Nakamura,K., Okamoto,A., Katou,Y., Yadani,C., Shitanda,T., Kaweeteerawat,C., Takahashi,T.S., Itoh,T., Shirahige,K., Masukata,H. *et al.* (2008) Rad51 suppresses gross chromosomal rearrangement at centromere in *Schizosaccharomyces pombe*. *EMBO J.*, **27**, 3036–3046.
43. Morin,I., Ngo,H.P., Greenall,A., Zubko,M.K., Morrice,N. and Lydall,D. (2008) Checkpoint-dependent phosphorylation of Exo1 modulates the DNA damage response. *EMBO J.*, **27**, 2400–2410.
44. Moss,J., Tinline-Purvis,H., Walker,C.A., Folkes,L.K., Stratford,M.R., Hayles,J., Hoe,K.L., Kim,D.U., Park,H.O., Kearsey,S.E. *et al.* (2010) Break-induced ATR and Ddb1-Cul4(Cdt)(2) ubiquitin ligase-dependent nucleotide synthesis promotes homologous recombination repair in fission yeast. *Genes Dev.*, **24**, 2705–2716.
45. Liu,C., Poitelea,M., Watson,A., Yoshida,S.H., Shimoda,C., Holmberg,C., Nielsen,O. and Carr,A.M. (2005) Transactivation of *Schizosaccharomyces pombe* cdt2+ stimulates a Pcu4-Ddb1-CSN ubiquitin ligase. *EMBO J.*, **24**, 3940–3951.
46. Liu,C., Powell,K.A., Mundt,K., Wu,L., Carr,A.M. and Caspari,T. (2003) Cop9/signalosome subunits and Pcu4 regulate ribonucleotide reductase by both checkpoint-dependent and -independent mechanisms. *Genes Dev.*, **17**, 1130–1140.
47. Aylon,Y. and Kupiec,M. (2003) The checkpoint protein Rad24 of *Saccharomyces cerevisiae* is involved in processing double-strand break ends and in recombination partner choice. *Mol. Cell. Biol.*, **23**, 6585–6596.
48. Dubrana,K., van Attikum,H., Hediger,F. and Gasser,S.M. (2007) The processing of double-strand breaks and binding of single-strand-binding proteins RPA and Rad51 modulate the formation of ATR-kinase foci in yeast. *J. Cell Sci.*, **120**, 4209–4220.
49. Zubko,M.K., Guillard,S. and Lydall,D. (2004) Exo1 and Rad24 differentially regulate generation of ssDNA at telomeres of *Saccharomyces cerevisiae* cdc13–1 mutants. *Genetics*, **168**, 103–115.
50. Zhu,Z., Chung,W.H., Shim,E.Y., Lee,S.E. and Ira,G. (2008) Sgs1 helicase and two nucleases Dna2 and Exo1 resect DNA double-strand break ends. *Cell*, **134**, 981–994.
51. Mimitou,E.P. and Symington,L.S. (2009) DNA end resection: Many nucleases make light work. *DNA Repair (Amst)*. **8**, 983–995.

52. Hu,J., Sun,L., Shen,F., Chen,Y., Hua,Y., Liu,Y., Zhang,M., Hu,Y., Wang,Q., Xu,W. *et al.* (2012) The intra-S phase checkpoint targets Dna2 to prevent stalled replication forks from reversing. *Cell*, **149**, 1221–1232.
53. Navadgi-Patil,V.M. and Burgers,P.M. (2009) A tale of two tails: activation of DNA damage checkpoint kinase Mec1/ATR by the 9-1-1 clamp and by Dpb11/TopBP1. *DNA Repair (Amst)*, **8**, 996–1003.
54. Xu,H., Boone,C. and Brown,G.W. (2007) Genetic dissection of parallel sister-chromatid cohesion pathways. *Genetics*, **176**, 1417–1429.
55. Covo,S., Westmoreland,J.W., Gordenin,D.A. and Resnick,M.A. (2010) Cohesin Is limiting for the suppression of DNA damage-induced recombination between homologous chromosomes. *PLoS Genet*, **6**, e1001006.
56. Fang,Y., Tsao,C.C., Goodman,B.K., Furumai,R., Tirado,C.A., Abraham,R.T. and Wang,X.F. (2004) ATR functions as a gene dosage-dependent tumor suppressor on a mismatch repair-deficient background. *EMBO J.*, **23**, 3164–3174.
57. Ward,I.M., Difilippantonio,S., Minn,K., Mueller,M.D., Molina,J.R., Yu,X., Frisk,C.S., Ried,T., Nussenzweig,A. and Chen,J. (2005) 53BP1 cooperates with p53 and functions as a haploinsufficient tumor suppressor in mice. *Mol. Cell. Biol.*, **25**, 10079–10086.
58. Lam,M.H., Liu,Q., Elledge,S.J. and Rosen,J.M. (2004) Chk1 is haploinsufficient for multiple functions critical to tumor suppression. *Cancer Cell*, **6**, 45–59.
59. Ira,G., Pellicioli,A., Balijja,A., Wang,X., Fiorani,S., Carotenuto,W., Liberi,G., Bressan,D., Wan,L., Hollingsworth,N.M. *et al.* (2004) DNA end resection, homologous recombination and DNA damage checkpoint activation require CDK1. *Nature*, **431**, 1011–1017.
60. Boutros,R., Lobjois,V. and Ducommun,B. (2007) CDC25 phosphatases in cancer cells: key players? Good targets? *Nat. Rev. Cancer*, **7**, 495–507.